05,07

Resonant studies of the effect of Bi^{3+} impurity on magnetic anisotropy and phase diagrams in gadolinium ferroborate $GdFe_3(BO_3)_4$

© A.I. Pankrats[1], S.A. Skorobogatov[1,2], I.N. Khoroshiy[1], S.M. Zharkov[1,2], G.M. Zeer[2], I.A. Gudim[1], V.R. Titova[1]

[1] Kirensky Institute of Physics,
Federal Research Center KSC Siberian Branch Russian Academy of Sciences (SB RAS) —
„Krasnoyarsk Scientific Center of SB RAS“,
Krasnoyarsk, Russia
[2] Siberian Federal University,
Krasnoyarsk, Russia

E-mail: pank@iph.krasn.ru

Received July 11, 2025
Revised October 1, 2025
Accepted October 13, 2025

The resonant properties of gadolinium ferroborate $GdFe_3(BO_3)_4$ single crystals of varying quality are compared: nominally pure and those containing Bi^{3+} ion impurities. The EDS method determined that the actual bismuth impurity content is close to the previously estimated 6% based on magnetic studies. The resonance properties confirm that both crystals form similar magnetic phase diagrams with an orientational transition between easy-axis and easy-plane antiferromagnetic ordering, which occurs either as a spontaneous transition at temperature T_{SR} or as a transition to a magnetic field-induced easy-plane state at $T < T_{SR}$. Temperature dependencies of the effective magnetic anisotropy fields and the magnetoanisotropic contributions of the iron and gadolinium subsystems are calculated from the resonance data. It is concluded that the Bi^{3+} ion impurity not only suppresses the contribution of the gadolinium subsystem, which these ions partially replace, but also causes a reduction in the contribution of the iron subsystem. As a result, the total change in the effective anisotropy field of the crystal is rather weak.

Keywords: magnetic anisotropy, resonance properties, magnetic phase diagrams, rare-earth ferroborates

DOI: 10.61011/PSS.2025.11.62958.186-25

1. Introduction

For the last couple decades the interest continues to grow in the study of physical properties of rare-earth (RE) borates with the huntite structure $RM_3(BO_3)_4$ (R = Y, La–Lu; M = Fe, Cr, Al, Ga), which crystallize in a non-centrosymmetric spatial group $R32$ or $P3_121$. This interest is explained not only by their non-linear-optical [1–3] and multiferroic [4–6] properties, but a rich spectrum of magnetic structures that this class of compounds demonstrates for M = Fe, Cr. Depending on the ion R^{3+} crystals may show the properties of simple antiferromagnetics with the antiferromagnetic axis oriented either along the trigonal axis of the crystal (–EA — easy axis of anisotropy for R = Tb, Dy, Pr [7–9]), or perpendicular to it in the basal plane (–EP — easy plane of anisotropy for R = Sm, Er, Eu [6,9]). For some RE ions the results of elastic neutron scattering and magnetic resonance X-ray spectroscopy demonstrate weak noncollinearity (R = Er [9] and Ho [10]) or incommensurable nature of the magnetic structure (R = Nd [11] and Gd above 10 K [12]).

Such wide spectrum of magnetic structures is due to the coexistence of two magnetic subsystems in the crystal. The studies of antiferromagnetic resonance (AFMR) and elastic neutron scattering of $YFe_3(BO_3)_4$ crystal containing only a subsystem of iron ions [10,13] demonstrated that the magnetic subsystem of Fe^{3+} ions is characterized by EP of anisotropy and at Néel temperature $T_N = 38$ K the magnetic moments of ions are ordered antiferromagnetically in the basal plane. The subsystem of RE ions, whose own exchange interaction is small, is ordered antiferromagnetically due to 3d-4f exchange interaction from the side of the iron subsystem. As a result of this interaction the RE subsystem makes its contribution to the total anisotropy of the crystal. Depending on the sign and value of the constant of the RE ion magnetic anisotropy this contribution either strengthens the EP anisotropy of the iron subsystem or competes therewith providing for a wide spectrum of possible magnetic structures.

The most interesting and promising situation for the study of orientation magnetic transitions in these crystals is the situation when the competing contributions of R^{3+}- and Fe^{3+}-subsystems to the magnetic anisotropy of the crystal are close in their absolute value. In this case the difference in the temperature dependences of the subsystem contributions may cause mutual compensation of contributions at a certain temperature and change in the sign of the total magnetic anisotropy causing a spontaneous orientation EA–EP transition. Besides, the weak dependence of RE ion magnetic anisotropy on the magnetic field against a

backdrop of nearly compensated total anisotropy may cause the orientation transition not only by temperature, but also in case of the magnetic field change. This is exactly the case with the competition of contributions of RE ions and Fe^{3+} subsystem in the RE gadolinium [13,14] and holmium ferroborates [10,15]. In diamagnetically diluted crystals $Pr_{1-x}Y_xFe_3(BO_3)_4$ at intermediate yttrium concentrations a similar mutual compensation of magnetoanisotropic contributions is also found, as well as the orientation transition between the EA and EP states induced by the magnetic field [16].

The AFMR method with its high sensitivity to the magnetic structure of the crystal is a unique tool for the study of the magnetic structures and phase transitions between various states. This method was first used for the crystals of the RE ferroborate group to study the magnetic structure and phase diagram of gadolinium ferroborate $GdFe_3(BO_3)_4$ [13,14]. In these papers it was shown, using the analysis of frequency-field dependences of AFMR, that below the Néel temperature $T_N = 38$ K the crystal demonstrates the established EP antiferromagnetic ordering with magnetic moments of Fe^{3+} and Gd^{3+} ions in the basal plane of the crystal. Further cooling was accompanied with spontaneous orientation transition from EP to EA antiferromagnetic structure at the temperature of $T_C \approx 8.5$ K. It was shown that this transition was caused by a change in the sign of the total magnetic anisotropy, and the temperature dependence of the contribution of the gadolinium ion subsystem to the magnetic anisotropy of the crystal was calculated from comparison with the resonance properties of yttrium ferroborate.

Single crystals $GdFe_3(BO_3)_4$, which were used for resonance studies in papers [13,14], were grown by the solution-melt method using a solvent $Bi_2Mo_3O_{12}$-B_2O_3 [17]. The recent paper [18] conducted the comparative analysis of the magnetic properties and phase diagrams „magnetic field–temperature“ for $GdFe_3(BO_3)_4$ crystals grown from three different solvents, and it was found that the most chemically pure were the single crystals obtained from the solvent based on lithium tungstate Li_2WO_4-B_2O_3. These crystals demonstrate the highest values of temperature of the spontaneous orientation transition $T_C \approx 10.5$ K. The strongest differences of magnetic phase diagrams for the magnetic fields $\mathbf{H} \parallel \mathbf{C}$ and $\mathbf{H} \perp \mathbf{C}$ were found in the crystals grown basing on the trimolybdate-bismuth solvent. The authors relate these changes to the uncontrolled admixtures Bi^{3+}, substituting up to ~ 6 at.% gadolinium ions.

The objective of this paper is the comparative study of AFMR, magnetic anisotropy and phase diagrams in the $GdFe_3(BO_3)_4$ crystals grown from solvents based on lithium tungstate Li_2WO_4-B_2O_3 and bismuth trimolybdate $Bi_2Mo_3O_{12}$. The resonance data were used to calculate the temperature dependences of the effective fields of magnetic anisotropy and magnetoanisotropic contributions of the iron and gadolinium subsystems. The conclusion was drawn that the admixture of ions Bi^{3+} not only suppressed the contribution of the gadolinium subsystem, which these ions partially substituted, but also caused the reduction of the iron subsystem contribution.

2. Samples and experimental procedure

The resonance experiments were conducted on single crystals $GdFe_3(BO_3)_4$, grown on the seed by the solution-melt method from solvents based on lithium tungstate Li_2WO_4 and bismuth trimolybdate $Bi_2Mo_3O_{12}$, the single crystal growth technology is described in paper [18]. The reagents of the following qualification were used for synthesis: Fe_2O_3 and B_2O_3 — (the content of the pure compound is 99.3 %), Gd_2O_3 — (the content of the admixture of other RE oxides does not exceed 0.01 %), solvents Li_2WO_4 — (97.1 %) and $Bi_2Mo_3O_{12}$ — (97.1 %). In all cases the quantity of admixtures critical for stoichiometry in the reagents is the fractions of percent and may not impact the stoichiometry of the grown crystals. To control the elemental composition of the single-crystal samples, a local elemental composition was studied using a scanning electron microscope (SEM) JEOL JSM-7001F with an energy-dispersive X-ray spectrometer (EDS) Oxford Inca PentaFetx3. Since the crystals are dielectrics, a layer of aluminum with thickness of 20 nm was sputtered to enable research on the sample surface under high vacuum. These studies demonstrated that in the crystals synthesized from lithium tungstate there were no admixtures of foreign elements and confirmed high stoichiometry of the chemical composition of single crystals, and the deviations from the perfect stoichiometry were within the method error. For a crystal synthesized from bismuth trimolybdate, the EDS-analysis confirmed that the only foreign admixture in this crystal was bismuth. The elemental solution of this single-crystal sample will be discussed in section 4.

Bulk transparent crystals of green color had the shape of a hexagonal prism with well-developed facets. In some crystals the top of the prism had a facet in the form of a regular triangle, the plane of which matched the basal one. The crystals were oriented in accordance with their habitus.

For resonance studies of the crystals grown from the solvent based on Li_2WO_4, two of the highest quality single crystals were chosen with maximum dimensions ~ 1 and 2 mm with the correct habitus and without foreign admixtures. Resonance properties of both crystals coincided fully, therefore the main measurements were made on the smallest sample with weight of 2.0 mg, having a smooth single resonant line in the entire studied frequency range. The width of the resonance line did not exceed 300 Oe in the frequency range of 26 GHz, such narrow line of AFMR confirmed the high quality of the crystal. The resonance lines for the second sample with weight of around 5 mg at low frequencies had the width of the same order as in the small sample. However, at frequencies above ~ 45 GHz additional peaks appeared in the resonance spectrum, and the main line widened due to inhomogeneity

of the microwave field in the large-size crystal. This sample was used in the measurements requiring higher sensitivity.

For a single crystal $GdFe_3(BO_3)_4$ synthesized from a solvent based on bismuth trimolybdate, partially the resonance data published previously in [14] was used. To collect additional data, the same single crystal was used as the one studied before in [13,14].

The studies of the antiferromagnetic resonance (AFMR) were carried out using an original spectrometer of magnetic resonance that operated in a wide frequency range (25–140 GHz) and pulsed magnetic field up to 90 kOe [19]. To control magnetic phase diagrams, magnetic static properties were measured using PPMS-9 Physical Property Measurement System, enabling measurements in the temperature range of 2–300 K and in the magnetic field of up to 90 kOe.

3. Experimental results

For certainty we will use designation $GdFe_3(BO_3)_4$ for single crystals synthesized from lithium tungstate, considering them nominally pure. We will designate crystals grown using bismuth trimolybdate and containing Bi impurities as $GdFe_3(BO_3)_4:Bi$.

Main frequency-field and temperature dependences of AFMR presented here for a single crystal $GdFe_3(BO_3)_4$ are taken from our paper [20]. For a single crystal $GdFe_3(BO_3)_4:Bi$ we both used the resonance data published previously in [13,14] and data obtained in process of this paper preparation.

First of all, note that no fundamental differences were found in the resonance properties of single crystals $GdFe_3(BO_3)_4$ grown using two different solvents. All differences are of quantitative nature, which is quite expectable.

3.1. Magnetic field H || C

Figure 1 shows frequency-field dependences of AFMR for both crystals measured at temperature $T = 4.2$ K in the magnetic field $\mathbf{H} \parallel \mathbf{C}$. Two areas may clearly be distinguished in this dependence. In the area of small magnetic fields for each crystal there are two branches of oscillations (*1* and *1′*), frequencies of which linearly depend on the field, and line widths for both samples do not exceed 300 Oe in the frequency range of 26 GHz. The boundaries of these areas in the field in Figure 1 are marked with narrow bands of pink and blue colors for $GdFe_3(BO_3)_4$ and $GdFe_3(BO_3)_4:Bi$ crystals, respectively. Comparison of the resonance properties of crystals shows that purer crystals $GdFe_3(BO_3)_4$ have higher values of the gap in the spectrum, and higher boundary values of the field, where the resonance absorption disappears for the branch *1*.

It is obvious that the type of frequency-field dependences of AFMR in this area for branches *1* and *1′* is specific for EA of antiferromagnetic state [21] in the fields that are

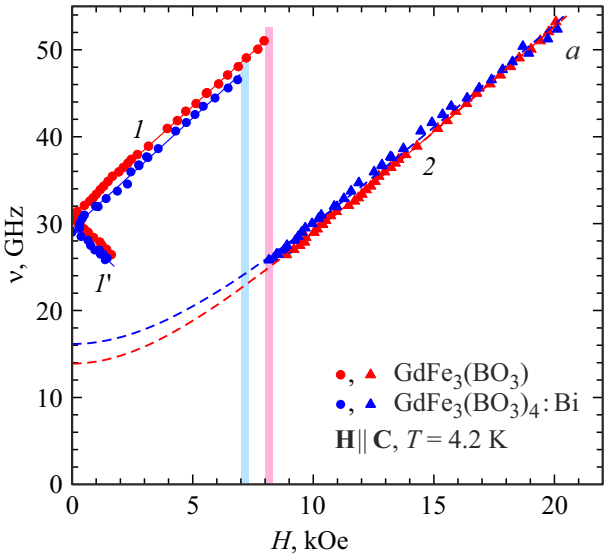

Figure 1. Frequency-field dependences of AFMR in single crystals $GdFe_3(BO_3)_4$ (taken from [20]) and $GdFe_3(BO_3)_4:Bi$ (taken from [14]) at $T = 4.2$ K, in magnetic field $\mathbf{H} \parallel \mathbf{C}$.

smaller than the spin-flip fields:

$$\frac{\upsilon_{1,2}}{\gamma_{\parallel}} = [(2H_E + H_A)H_A]^{1/2} \pm H, \qquad (1)$$

where $\upsilon_{\parallel c}^{EA} = \gamma_{\parallel} H_{\triangle} = [(2H_E + H_A)H_A]^{1/2}$ — gap in the spectrum.

Resonance parameters for both crystals at $T = 4.2$ K have the following values:

$\upsilon_{\parallel c}^{EA} = (31.0 \pm 0,1)$ GHz and $\gamma_{\parallel} = (2.60 \pm 0.05)$ GHz/kOe

for $GdFe_3(BO_3)_4$.

$\upsilon_{\parallel c}^{EA} = (29.4 \pm 0,2)$ GHz and $\gamma_{\parallel} = (2.55 \pm 0.05)$ GHz/kOe

for $GdFe_3(BO_3)_4:Bi$.

Let us consider in more detail the high-frequency area of the oscillation branch *1* in the $GdFe_3(BO_3)_4$ crystal. Figure 2 shows transformation of the resonance spectrum approaching the boundary of the EA state area. In frequencies 48.05 and 49.05 GHz the resonance fields are still rather far from the boundary of existence of the state EA shown with a vertical dotted line. In these frequencies, and in the boundary frequency of 50.07 GHz, the resonance lines are observed fully. In frequency 51.03 GHz a part of the resonance line disappears in the area of the field-induced spin-reorientation transition. With further frequency increase the resonance absorption for this branch totally disappears. In frequency 52.08 GHz only a non-resonant response is observed — a weak anomaly provided for by the response of the reflected microwave signal to the change in the crystal magnetic structure. In some other frequencies similar weak anomalies marked with an asterisk are also noticeable against the background of the intense main resonance line.

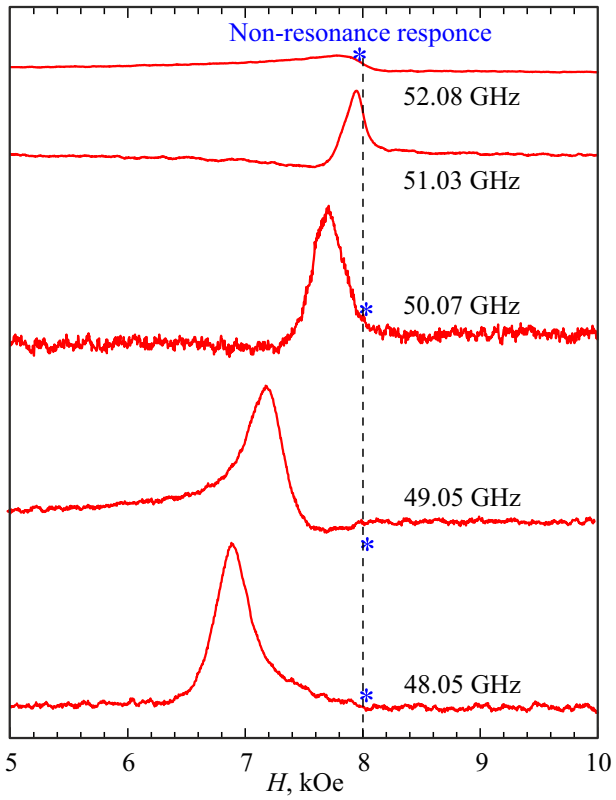

Figure 2. AFMR spectra in EA phase in $GdFe_3(BO_3)_4$ at different frequencies. $T = 4.2$ K, **H** ∥ **C**.

In the area of the fields above the boundary in both crystals there is a resonance branch *2*, which looks specific for the EP of the antiferromagnetic state, which at $T = 4.2$ K is induced by magnetic field. Frequency-field dependence of AFMR for this branch is as follows [21]:

$$\left(\frac{\upsilon_{\|1}}{\gamma_{\|}}\right)^2 = 2H_E\,|H_A| + H^2, \qquad (2)$$

$$\upsilon_{\|2=0}$$

Here $H_A < 0$ — field of anisotropy in the induced EP state. Dotted lines in Figure 1 for a branch of oscillations *2* correspond to this equation with values of energy gap $\upsilon_{\|c}^{EP} = \gamma_{\|}\sqrt{2H_E|H_A|} = (13.9 \pm 0.4)$ GHz for $GdFe_3(BO_3)_4$ and $\upsilon_{\|c}^{EP} = (16.5 \pm 0.5)$GHz for $GdFe_3(BO_3)_4$:Bi. The second branch of AFMR $\nu_{\|2}$ in this state is Goldstone mode.

In papers [13,14] it was shown that in a gadolinium ferroborate crystal the spontaneous orientation transition of EA–EP is due to the difference in temperature dependences for the competing magnetoanisotropic contributions of gadolinium and iron subsystems. Therefore, study of the temperature dependences of this crystal resonance parameters play a critical role, since against the background of nearly compensated effective magnetic anisotropy of the crystal the uncontrolled impurities may have a noticeable effect at its phase diagram.

Temperature dependences of resonance fields of AFMR in $GdFe_3(BO_3)_4$ and $GdFe_3(BO_3)_4$:Bi single crystals measured at different frequencies are shown in Figure 3. In this dependence you can also identify the resonance data related to the EA (lines *1* and *1′*) and EP (lines *2*) states. In the EA state, if measured at all frequencies above the gap $\nu_{\|c}$, the resonance field increases with the temperature growth, this is explained by decrease of the gap caused by decrease of the effective field of crystal anisotropy. The corresponding temperature dependence of the gap ν_c calculated from this data for the EA state is given in Figure 4. More complex

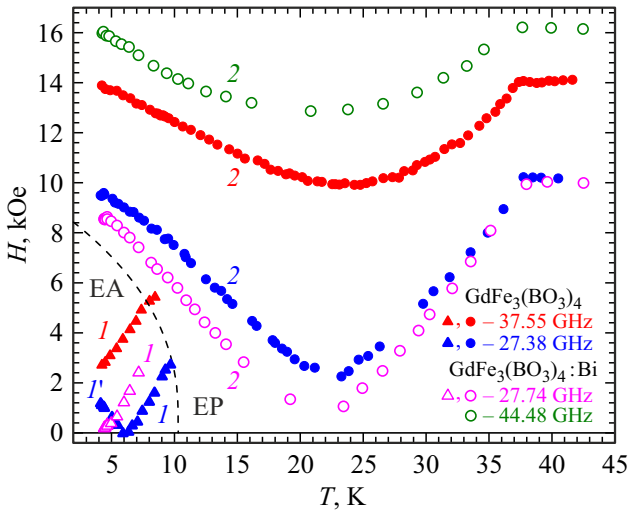

Figure 3. Temperature dependences of resonance fields of AFMR in $GdFe_3(BO_3)_4$ (closed symbols) and $GdFe_3(BO_3)_4$:Bi (open symbols) single crystals at **H** ∥ **C**. Figures in dependences correspond to the designations of the oscillation branches in Figure 1. The dashed line shows a phase boundary of EA–EP taken from paper [18].

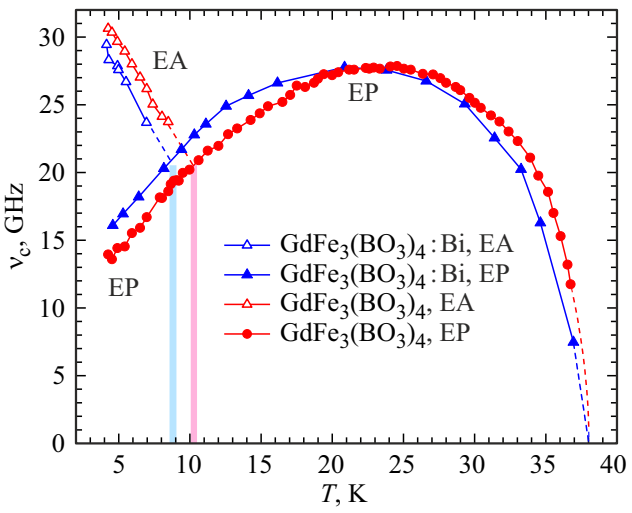

Figure 4. Temperature dependences of energy gaps in the spectrum for EA and EP states measured in $GdFe_3(BO_3)_4$:Bi and $GdFe_3(BO_3)_4$ in frequencies of 27.74 GHz and 37.55 GHz, respectively.

dependence for the resonance field when measured at the frequency of 27.38 GHz for $GdFe_3(BO_3)_4$, lower than the value $\nu_{\|c}$ for $T = 4.2$ K is caused by the fact that with the growth of temperature and decrease of the gap, a transition from the line *1′* (Figure 1) to the frequency-field dependence 1 occurs. Note that for any frequency the maximum values of the resonance field observed in the EA state are actually the critical fields of transition between the EA and EP states.

Temperature dependences of resonance fields in the EP state when heated decrease first with the minimum in the area of 20–25 K, then increase to the values of the resonance field in the paramagnetic state approaching the temperature of $T_N = 38$ K. The corresponding non-monotonic dependences of energy gaps for this state are also given in Figure 4 for both crystals. Temperature areas of spontaneous EA–EP reorientation in this figure are indicated with the blue and pink strips for $GdFe_3(BO_3)_4$:Bi and $GdFe_3(BO_3)_4$, respectively. At temperatures below the reorientation areas in both crystals the EP state is induced by the magnetic field.

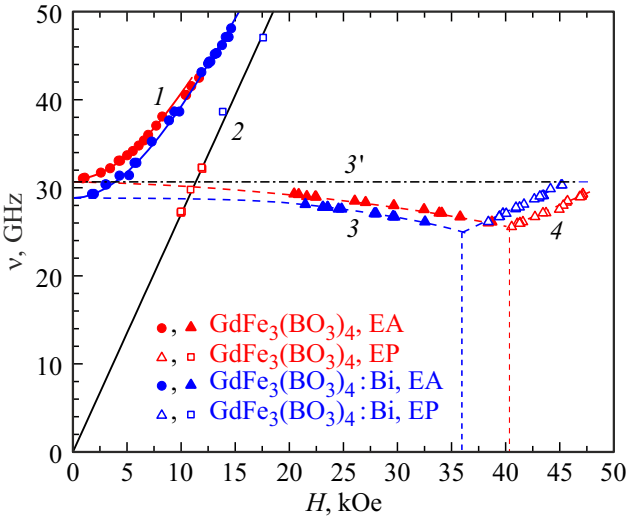

Figure 5. Frequency-field dependences of AFMR in single crystals $GdFe_3(BO_3)_4$ (taken from [20]) and $GdFe_3(BO_3)_4$:Bi (taken from [14]) in magnetic field $\mathbf{H} \perp \mathbf{C}$, $T = 4.2$ K for curves *1, 3* and *4*. The points in the curve *2* were obtained at temperatures of $T > T_{SR}$.

3.2. Magnetic field $\mathbf{H} \perp \mathbf{C}$

The conclusion on formation of the EA state in the area of low temperatures and small magnetic fields is confirmed by resonance properties as well in the field oriented in the basal plane of the crystal. Frequency-field dependences of AFMR in $GdFe_3(BO_3)_4$ and $GdFe_3(BO_3)_4$:Bi single crystals for this field orientation are shown in Figure 5.

If the effective anisotropy is rather weak, $H_A \ll H_E$, which is implemented well in gadolinium ferroborate, the frequency-field dependences have the following form [21]:

$$\left(\frac{\nu_{\perp 1}}{\gamma_\perp}\right)^2 = (2H_E + H_A)H_A + \frac{2H_E - H_A}{2H_E + H_A}H^2 \approx (2H_E + H_A)H_A + H^2,$$

$$\left(\frac{\nu_{\perp 2}}{\gamma_\perp}\right)^2 = (2H_E + H_A)H_A - \frac{H_A}{2H_E + H_A}H^2. \qquad (3)$$

Oscillations of both branches (3) are characterized by the same value of the energy gap and are degenerate at $H = 0$.

Curves *1* for both crystals are described well by the first equation with the following parameters:

$\gamma_\perp = (2.65 \pm 0.02)$ GHz/kOe and $\nu_{\perp c} = (31.0 \pm 0.1)$ GHz

for $GdFe_3(BO_3)_4$ and

$\gamma_\perp = (2.66 \pm 0.02)$ GHz/kOe and $\gamma_\perp = (29.0 \pm 0.2)$ GHz

for $GdFe_3(BO_3)_4$:Bi. In both crystals the $\nu_{\perp c}$ values match the corresponding $\nu_{\|c}$ values for $\mathbf{H} \parallel \mathbf{C}$ orientation.

In $\mathbf{H} \perp \mathbf{C}$ orientation you can also observe both the spontaneous reorientation EA–EP transition by temperature and the one induced by magnetic field [14,18]. In EP state the frequency-field dependences of AFMR with neglection of weak (according to AFMR data) magnetic anisotropy in the basal plane have the following form [21]:

$$\frac{\nu_{\perp 1}}{\gamma_\perp} = H\sqrt{1 + \frac{|H_A|}{2H_E}} \approx H$$

$$\left(\frac{\nu_{\perp 2}}{\gamma_\perp}\right)^2 = 2H_E|H_A| - \frac{|H_A|}{2H_g}H^2. \qquad (4)$$

At $T = 4.2$ K no oscillations of branch $\nu_{\perp 1}$ are observed, since in the frequency range studied in the experiment the resonance values of the fields are below the critical ones that are necessary for transition into the EP induced state. Figure 5 presents the experimental points for this branch *2*, measured for both crystals at temperatures above the temperature of the spontaneous EA–EP transition.

Let us consider the resonance properties of crystals in EA and EP states that are described by the second branches of $\nu_{\perp 2}$ oscillations in equations (3) and (4) and occupy the frequency range below the energy gap. Note that at $H_A \ll H_E$ the functional dependences of $\nu_{\perp 2}$ oscillation frequencies on the applied magnetic field in both states agree fully. Under the same condition in both states the resonance frequencies $\nu_\perp$ in the area of small fields exhibit a very weak dependence on the applied field, the steepness of this dependence is determined by the ratio $H_A/2H_E$ for EA or $|H_A|/2H_E$ for EP states. According to the estimates for the gadolinium ferroborate, this ratio does not exceed $\sim 10^{-4}$. In conventional antiferromagnetics the noticeable softening of the frequency in $\nu_{\perp 2}$ appears only when approaching the field $H \approx 2H_E$, and at the scale of Figure 5 the theoretical frequency-field dependence for the branch $\nu_{\perp 2}$ is shown

with the horizontal dashed-dotted line *3′*. Due to weak field dependence, the resonance absorption for these branches is usually not detected in the small magnetic fields when using the field sweep. However, the experiment shows a rather strong dependence of resonance frequencies 3 and 4 on the applied magnetic field. For the first time this result was found in paper [14] when studying AFMR in the crystals of gadolinium ferroborate $GdFe_3(BO_3)_4$: Bi. Such strong dependence was explained by the fact that the effective magnetic anisotropy and, accordingly, the energy gap depends on the applied magnetic field.

Note that the frequency-field dependence in this area of the spectrum has a specific form: as the field increases, the resonance frequency first decreases nearly linearly, then, starting from a certain critical field H_c, its nearly linear growth is observed. It is obvious that the kink of this dependence occurs due to the orientation EA–EP transition, the critical fields at $T = 4.2$ K are ~ 40.5 kOe and ~ 36 kOe, accordingly, for $GdFe_3(BO_3)_4$ and $GdFe_3(BO_3)_4$: Bi. Therefore, the branch of oscillations *3* in Figure 5 corresponds to oscillations $\nu_{\perp 2}$ in the EA state and is described by the second equation in (3), and the branch of oscillations *4* is described by the second equation for $\nu_{\perp 2}$ in (4) and corresponds to the oscillations in the EP state.

When temperature dependence of resonance fields are measured at $\mathbf{H} \parallel \mathbf{C}$, it was noted that for any frequency the maximum values of the resonance field observed in the EA state are actually the critical fields of transition between the EA and EP states. Figure 6 shows temperature dependences of critical fields for a $GdFe_3(BO_3)_4$ single crystal obtained from AFMR spectrum and magnetic measurements at PPMS at the same sample (with weight of 2 mg) with the magnetic field orientation along the crystal trigonal axis. The data of the magnetic measurements are close to the dependence in paper [18] shown in the figure with the dashed line, which is approximation of the dependence for the experimental points using the power law.

At the same time the resonance measurements do show a similar dependence, but yield values of critical fields that are noticeably higher than those obtained from the magnetic measurements. Apart from the causes for such difference that are conventional for using different experimental methods (different samples, different methods to determine the transition moment, unavoidable errors of measurement etc.), it seems that the considerable contribution is made by the pulse nature of the magnetic field. This reorientation is the first-order transition, when in the critical area of temperatures an intermediate state is formed, where EA and EP phases co-exist. The dynamics of such transition depends on the speed of magnetic field change, which, when the field pulse duration of ~ 12 ms is used, is around $5 \cdot 10^6$ Oe/s, which is several orders of magnitude higher than in the magnetic measurements.

This figure shows the similar dependences for a $GdFe_3(BO_3)_4$: Bi single crystal. Experimental values of the critical fields obtained from AFMR spectra [14] match the

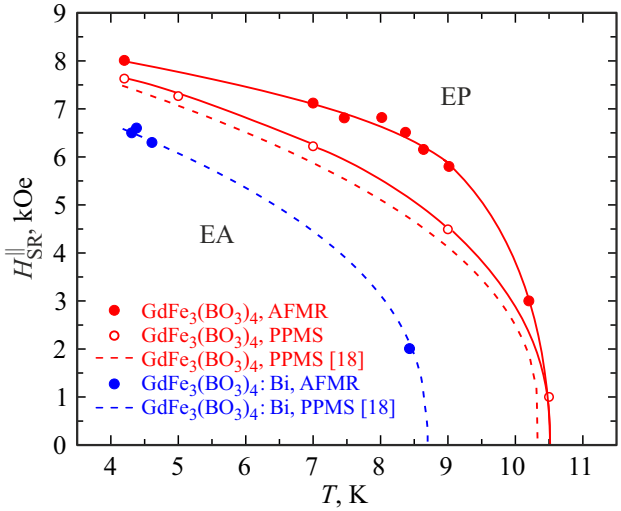

Figure 6. Temperature dependence of critical fields of the orientation EA –EP transition in $GdFe_3(BO_3)_4$ single crystals and $GdFe_3(BO_3)_4$: Bi, $\mathbf{H} \parallel \mathbf{C}$. Dashed lines data [18] (see notes in the text).

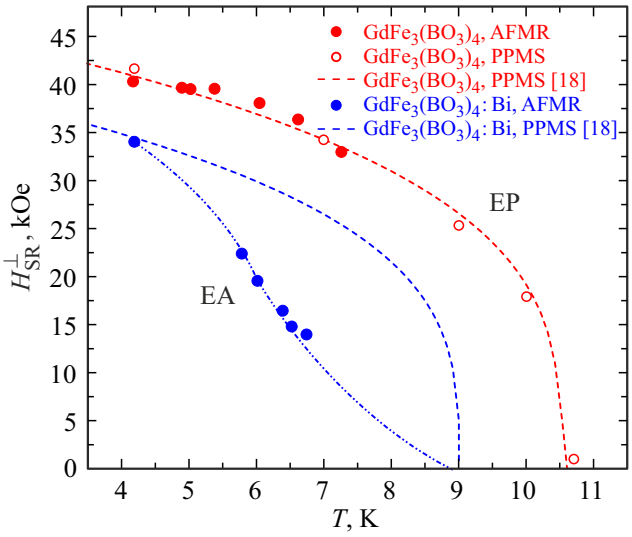

Figure 7. Temperature dependence of critical fields of the orientation EA –EP transition in $GdFe_3(BO_3)_4$ single crystals and $GdFe_3(BO_3)_4$: Bi, $\mathbf{H} \perp \mathbf{C}$. The dashed-dotted line is drawn „by eye“.

dashed curve that approximates using the power law the experimental dependence measured at PPMS [18].

Phase diagrams of $GdFe_3(BO_3)_4$ and $GdFe_3(BO_3)_4$: Bi crystals for the case of magnetization in the basal plane are shown in Figure 7. Critical fields of EA–EP transition in the $GdFe_3(BO_3)_4$ crystal are close to the ones measured in [18], even though in this case in the area of intermediate temperatures the resonance measurements show somewhat higher values of the critical fields than in magnetic measurements. Here the temperature dependences of critical fields are also shown for a $GdFe_3(BO_3)_4$: Bi crystal taken from

paper [18] (dashed curve), and the AFMR data [14]. The resonance data agrees well with the results of the magnetic measurements at $T = 4.2$ K and in area of spontaneous transition, but at intermediate temperatures the temperature dependences differ significantly. Even though it should be said that the comparison is carried out with approximation of the experimental dependence, and the experimental points are given in paper [18] only for temperatures of 4.2 K and in close proximity to the temperature of the spontaneous reorientation transition, and no points are present in the intermediate area of temperatures. Therefore, the issue of comparing the phase boundaries in the $GdFe_3(BO_3)_4$:Bi crystal obtained by the resonance [13,14] and magnetostatic [18] methods remains open.

4. Discussion

When analyzing the impact of Bi^{3+} ion impurity on magnetic anisotropy $GdFe_3(BO_3)_4$, it is reasonable to assume that the effective field of crystal anisotropy was due to the contributions of two magnetic subsystems of Fe^{3+} and Bi^{3+} ions. In paper [18] an assumption was made that the effect of impurity ions Bi^{3+} reduces only to the partial substitution in the gadolinium ion subsystem and does not effect the magnetic properties of the iron ion subsystem. Such approach makes it possible to calculate the contribution of Gd^{3+} to magnetic anisotropy, using the data for effective anisotropy of the crystal calculated from the energy gap of AFMR, and the data for the magnetic anisotropy of the iron subsystem obtained from AFMR in the $YFe_3(BO_3)_4$ crystal [13], containing only Fe^{3+} magnetic ions. At the same time it is important that the $YFe_3(BO_3)_4$ single crystal was grown using the same technology as $GdFe_3(BO_3)_4$:Bi, accordingly, and in this crystal the Bi^{3+} impurity ions partially substituted Y^{3+} ions in the corresponding positions.

Figure 8, *a* shows temperature dependences of effective anisotropy fields H_A for the $GdFe_3(BO_3)_4$ and for $GdFe_3(BO_3)_4$:Bi. Effective values of the crystal anisotropy fields were calculated from the temperature dependences of energy gaps (Figure 4) using expressions (1) and (2) using the exchange field for the iron subsystem $H_E = 700$ kOe at $T = 4.2$ K [13]. Usually, the dependence of the exchange field on temperature was described by the Brillouin function $B_{5/2}$. Note that our paper [13] provided such temperature dependence for the H_A field in the $GdFe_3(BO_3)_4$:Bi crystal that was a continuous function when transitioning through the orientation transition temperature. However, the thorough measurements for the $GdFe_3(BO_3)_4$ crystal and analysis of resonance data for $GdFe_3(BO_3)_4$:Bi demonstrated that in both crystals the effective field of anisotropy at the orientation transition undergoes a jump as shown in Figure 8, *a*. The origin for such jump-like behavior of the anisotropy field will be discussed in a separate article.

Based on the independence of the iron subsystem contribution on the bismuth impurity and temperature

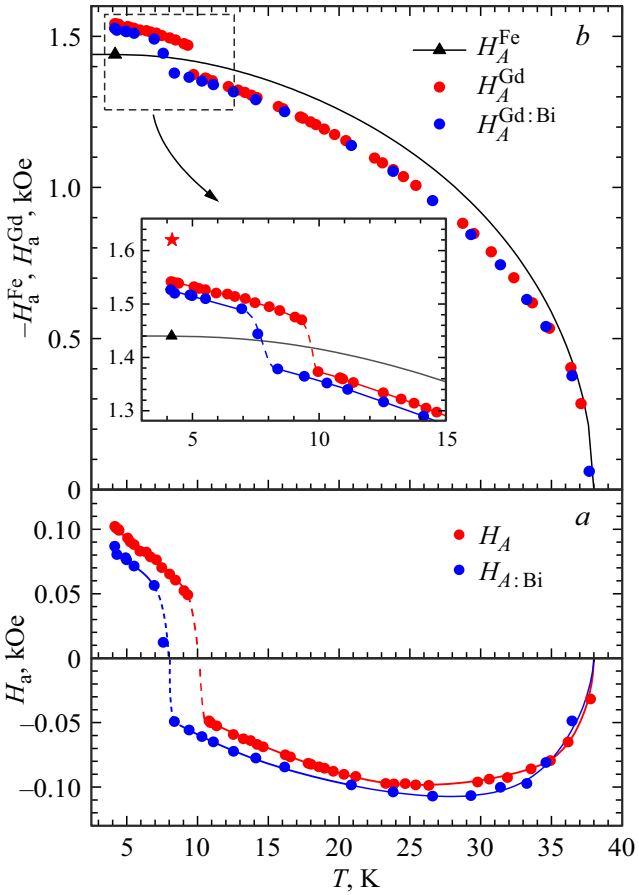

Figure 8. Temperature dependences: *a* — of effective fields of magnetic anisotropy H_A and *b* — magnetic-anisotropic contributions of iron — H_A^{Fe} and gadolinium H_A^{Gd} subsystems for $GdFe_3(BO_3)_4$ (red) and $GdFe_3(BO_3)_4$:Bi (blue).

dependences of effective fields of $GdFe_3(BO_3)_4$ and $GdFe_3(BO_3)_4$:Bi crystal anisotropy, we calculated the temperature dependences of the contribution of magnetoanisotropic contribution of the gadolinium subsystem, the results are shown in Figure 8, *b*. These calculations took into account the fact that the anisotropy field of the iron subsystem is $H_A^{Fe} = -1.44$ kOe at $T = 4.2$ K, and its temperature dependence is described well by the Brillouin function $B_{5/2}$ [13].

The table provides the values of effective fields of magnetic anisotropy H_A in $GdFe_3(BO_3)_4$ and $GdFe_3(BO_3)_4$:Bi crystals, and also effective fields of anisotropic contributions of iron and gadolinium subsystems at temperature $T = 4.2$ K. Comparison of the data shows that partial substitution with bismuth ions in the gadolinium subsystem of $GdFe_3(BO_3)_4$:Bi crystal caused decrease of the effective field of anisotropy of H_a crystal only by ~ 15 Oe. If at the same time the anisotropic properties of the iron subsystem are considered stable, such change in the crystal's effective anisotropy should be attributed to the decrease in the contribution of the gadolinium subsystem.

Effective anisotropy fields H_A of $GdFe_3(BO_3)_4$ and $GdFe_3(BO_3)_4:Bi$ crystals and effective anisotropy fields for the contributions of iron and gadolinium subsystems at temperature of $T = 4.2\,K$

Crystals	H_A, kOe	H_a^{Fe}	H_a^{Gd}, koe
$GdFe_3(BO_3)_4$	0.102	$-1.44(?)/-1.52^*$	$1.54/1.62^*$
$GdFe_3(BO_3)_4:Bi$, [13]	0.087	-1.44	1.52

Therefore, within the framework of this model, the decrease in the anisotropic contribution of the gadolinium subsystem in the $GdFe_3(BO_3)_4:Bi$ crystal due to impurity substitution does not exceed 1%. At the same time, according to the data from [18], up to 6 at.% of Gd^{3+} ions in these crystals are substituted by bismuth; consequently, the expected decrease in the anisotropic contribution of the gadolinium subsystem is several times greater than the estimate given above. Thus, it has been found that Bi^{3+} ion impurities lead to a change in the effective anisotropy field of gadolinium ferroborate that is several times weaker than the expected change in the anisotropic contribution of the gadolinium subsystem. There are two most likely reasons for this discrepancy: either the actual content of bismuth impurity in the crystal indeed does not exceed 1 at.%, or this impurity also suppresses the anisotropic contribution of the iron subsystem.

Content of Bi^{3+} ion impurity in a $GdFe_3(BO_3)_4:Bi$ single crystal, at which the measurements of AFMR were made [13], was determined using the EDS method. The spectra were surveyed in two adjacent facets of the sample, in general around 40 spectra were obtained. Based on the averaged data, the atomic proportion of element content was calculated in the $Gd_{0.96}Bi_{0.04}Fe_3(BO_3)_4$ sample. However, there is reason to believe that the bismuth content defined by the EDS method turned out to be slightly lower than the actual one due to the partial loss of the signal as a result of the sample surface irregularity (Figure 9). Most probably, the actual content of Bi^{3+} ion impurity in respect to the gadolinium atoms is close to the estimate of 6 at.% made on the basis of the magnetic measurements in single crystals from the same synthesis [18].

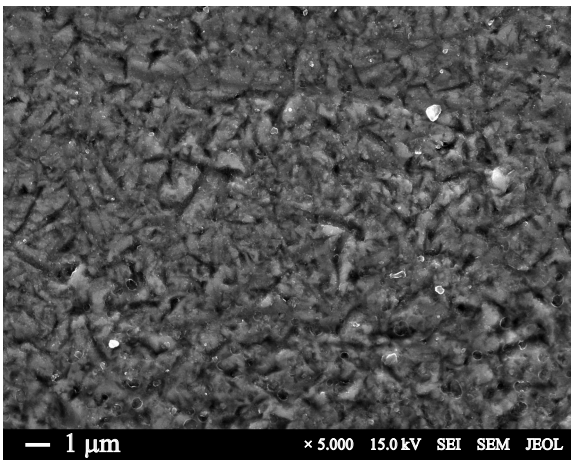

Figure 9. SEM image of sample surface $GdFe_3(BO_3)_4:Bi$.

The above analysis makes it possible to conclude the following. For $GdFe_3(BO_3)_4:Bi$ the given temperature dependence of the magnetoanisotropic contribution of gadolinium may be recognized as relevant, since all initial measurements were made on the crystals grown using the same technology and having the same quality according to impurity content. For $GdFe_3(BO_3)_4$ the given contribution of the gadolinium subsystem should probably be considered underestimated. In case of the bismuth impurity content at 6% in $GdFe_3(BO_3)_4:Bi$, the value of the anisotropic contribution of gadolinium in $GdFe_3(BO_3)_4$ may be estimated as $H_A^{Gd} = 1.62\,kOe$ at $T = 4.2\,K$. This value is noted with a red asterisk in the insert of Figure 8, *b*.

If the iron subsystem contribution at the same time did not depend on the bismuth impurity, from the chart you can see that the effective anisotropy field of the $GdFe_3(BO_3)_4$ crystal would nearly twice exceed the experimental value, and the spontaneous orientation transition would most probably be absent. Based on the experimental value of the effective field of crystal anisotropy, you can also estimate the magnetoanisotropic contribution of the iron subsystem $H_A^{Fe} = -1.52\,kOe$. Both assumed values of magnetoanisotropic contributions of subsystems for the $GdFe_3(BO_3)_4$ crystal are given in the table and are marked with an asterisk.

5. Conclusions

The paper compared the resonance properties of $GdFe_3(BO_3)_4$ gadolinium ferroborate crystals grown by solution-melt technology from solvents based on Li_2WO_4-B_2O_3 lithium tungstate and $Bi_2Mo_3O_{12}$ bismuth trimolybdate. Using the last solvent causes partial substitution of Gd^{3+} ions with Bi^{3+} ions. Using the EDS method, the content of bismuth impurity was found in the crystal synthesized using bismuth trimolybdate, it turned out to be close to the estimate of 6 at.% from the content of gadolinium made on the basis of magnetic studies. The resonance properties confirm that similar magnetic phase diagrams are formed in both crystals with the reorientation transition between easy-axis and easy-plane antiferromagnetic ordering, which is implemented either as a spontaneous transition at temperature of T_{SR} or as a transition to the easy-plane state induced by the magnetic field at $T < T_{SR}$. The data of the magnetic measurements is confirmed that the bismuth impurity causes decrease of temperature of the spontaneous reorientation transition between the states with easy-axis and easy-plane antiferromagnetic ordering, and also critical transition fields at $T < T_{SR}$. For both crystals the magnetic phase diagrams were built in the $\mathbf{H} \parallel \mathbf{C}$ and $\mathbf{H} \perp \mathbf{C}$ fields. It was found that in some cases the values of the critical transition

fields obtained from AFMR exceed the values measured by the magnetic static method. It is assumed that this effect is due to the high speed of field variation in the AFMR spectrometer with the pulsed magnetic field, which is important in the study of the first-order phase transitions.

Using temperature dependences of energy gaps in the AFMR spectrum, temperature dependences of effective magnetic anisotropy fields were calculated for both crystals. Based on the analysis of bismuth impurity impact at the effective anisotropy fields of crystals and magnetic-anisotropic contributions of magnetic subsystems, the conclusion was made that the Bi^{3+} ion impurity did not only suppress the contribution of the gadolinium subsystem that these ions partially substituted, but also causes reduction in the iron subsystem contribution. As a result, the total change of the effective anisotropy field of the crystal turns out to be rather weak.

Funding

The study was carried out within the framework of the research topic of the State Assignment of the Institute of Physics of the Siberian Branch of the Russian Academy of Sciences. The authors are grateful to the Krasnoyarsk Regional Center for Collective Use, Krasnoyarsk Scientific Center, Siberian Branch of the Russian Academy of Sciences, for the opportunity to study the magnetic properties of crystals. SEM and EDS studies of the crystal were conducted in the Resource Sharing Center of the Siberian Federal University.

Conflict of interest

The authors declare that they have no conflict of interest.

References

[1] S.R. Chinn, H.Y.-P. Hung. Opt. Commun. **15**, *3*, 345 (1975).
[2] H.Y.-P. Hong, K. Dwight. Mater. Res. Bull. **9**, *12*, 1661 (1974).
[3] P. Dekker, J.M. Dawes, J.A. Pipper, Y. Liu, J. Wang. Opt. Commun. **195**, *5–6*, 431 (2001).
[4] A.K. Zvezdin, S.S. Krotov, A.M. Kadomtseva, G.P. Vorob'ev, Yu.F. Popov, A.P. Pyatakov, L.N. Bezmaternykh, E.A. Popova. JETP Lett. **81**, *6*, 272 (2005).
[5] A.K. Zvezdin, G.P. Vorob'ev, A.M. Kadomtseva, Yu.F. Popov, A.P. Pyatakov, L.N. Bezmaternykh, A.V. Kuvardin, E.A. Popova. JETP Lett. **83**, *11*, 600 (2006).
[6] A.M. Kadomtseva, Yu.F. Popov, G.P. Vorob'ev, A.P. Pyatakov, S.S. Krotov, K.I. Kamilov, V.Yu. Ivanov, A.A. Mukhin, A.K. Zvezdin, A.M. Kuz'menko, L.N. Bezmaternykh, I.A. Gudim, V.L. Temerov. Low Temp. Phys. **36**, *6*, 511, (2010).
[7] C. Ritter, A. Balaev, A. Vorotynov, G. Petrakovskii, D. Velikanov, V. Temerov, I. Gudim, J. Phys.: Condens. Matter **19**, *19*, 196227 (2007).
[8] I.A. Gudim, A.I. Pankrats, E.I. Dumaĭkin, G.A. Petrakovskiĭ, L.N. Bezmaternykh, R. Szymczak, M. Baran. Cryst. Rep. **53**, *7*, 1140 (2008).
[9] C. Ritter, A. Vorotynov, A. Pankrats, G. Petrakovskiĭ, V. Temerov, I. Gudim, R. Szymczak. J. Phys.: Condens. Matter **22**, *20*, 206002 (2010).
[10] C. Ritter, A. Vorotynov, A. Pankrats, G. Petrakovskiĭ, V. Temerov, I. Gudim, R. Szymczak. J. Phys.: Condens. Matter **20**, *36*, 365209 (2008).
[11] M. Janoschek, P. Fischer, J. Schefer, B. Roessli, V. Pomjakushin, M. Meven, V. Petricek, G. Petrakovskii, L. Bezmaternikh. Phys. Rev. B **81**, *9*, 094429 (2010).
[12] H. Mo, C.S. Nelson, L.N. Bezmaternykh, V.L. Temerov, Phys. Rev. B **78**, *21*, 214407 (2008).
[13] A.I. Pankrats, G.A. Petrakovskiĭ, L.N. Bezmaternykh, V.L. Temerov. Phys. Solid State **50**, *1*, 79 (2008).
[14] A.I. Pankrats, G.A. Petrakovskii, L.N. Bezmaternykh, O.A. Bayukov. JETP **99**, *4*, 766 (2004).
[15] A. Pankrats, G. Petrakovskii, A. Kartashev, E. Eremin, V. Temerov. J. Phys.: Condens. Matter **21**, *43*, 436001 (2009).
[16] A.I. Pankrats, S.M. Zharkov, G.M. Zeer, I.A. Gudim. J. Alloys Compd. **909**, *16*, 164821 (2022).
[17] L.N. Bezmaternykh, V.L. Temerov, I.A. Gudim, N.A. Stolbovaya. Crystallogr. Rep. **50**, S1, 97 (2005).
[18] E.V. Eremin, I.A. Gudim, V.R. Titova, Physics of the Solid State **65**, *11*, 1844 (2023).
[19] V.I. Tugarinov, I.Ya. Makievskii, A.I. Pankrats, Instrum. Exp. Tech. **47**, *4*, 472 (2004).
[20] I.N. Khoroshiy, S.A. Skorobogatov, S.E. Nikitin, I.A. Gudim, V.R. Titova, A.I. Pankrats, arXiv:2510.27458 [cond-mat.str-el] (2025).
[21] A.G. Gurevich, G.A. Melkov, Magnitniye kolebaniya i volny. Fizmatlit, M. (1994) (in Russian).

Translated by M.Verenikina